Demonstration of the evanescent Kerr effect in optical nanofibers

GIL FANJOUX,[1,*] JACQUES CHRÉTIEN,[1], ADRIEN GODET,[1], KIEN PHAN-HUY,[1], JEAN-CHARLES BEUGNOT,[1], AND THIBAUT SYLVESTRE[1]

[1] *Institut FEMTO-ST, UMR 6174 CNRS, Université Bourgogne Franche-Comté, 25030 Besançon, France*
[*] *gil.fanjoux@univ-fcomte.fr*

Abstract: Optical nanofibers have recently emerged as attractive nanophotonic platforms for many applications ranging from quantum technologies to nonlinear optics, due to both their tight optical confinement and their wide evanescent field. Herein we examine both theoretically and experimentally the optical Kerr effect induced by the evanescent field of a silica nanofiber surrounded by different nonlinear liquids such as water, ethanol and acetone and we further compare them with air cladding. Our results show that the evanescent Kerr effect significantly dominates the usual Kerr effect into the silica core for sub-wavelength diameters below 560 nm, using acetone. We further report the observation of the evanescent Kerr effect through surrogate measurements of stimulated Raman-Kerr scattering (SRKS) in an acetone-immersed silica nanofiber. Our findings open the way towards potential applications of optical nanofibers to ultra-sensitive liquid sensing or to enhancing the nonlinear effects through the evanescent field.

1. Introduction

Optical nanofibers are ultra-thin optical fibers manufactured by heating and stretching standard silica-based optical fibers down to submicron scale over a few centimeters [1]. These ultra-thin fibers have many optical properties that make them interesting for a number of applications including plasmonics, quantum and atom optics, optical sensing, and nonlinear photonics. Among the most important are the strong light confinement in the waist region, the wide evanescent field in the sub-wavelength limit, and the tailorable group-velocity dispersion [2–5]. These remarkable optical properties have been exploited in many key experimental demonstrations such as octave-spanning supercontinuum generation over short propagation distance [6], atom trapping in the evanescent field of the nanofiber [7, 8], ultra-sensitive chemical or biological sensors [9], high-Q micro-resonator coupling [10], and nanofiber-based interferometers and resonators [1]. They also possess exceptional mechanical and elastic properties that make them attractive for surface acoustic wave generation and Brillouin light scattering, as recently reported in ~~reference~~ [11]. Among third-order nonlinear effects, stimulated Raman scattering has recently been evidenced in the evanescent field of silica nanofibers dipped in ~~nonlinear Raman~~ liquid such as ethanol and toluene [12]. Although the evanescent field has already been exploited for enhancing nonlinear effects using metals and plasmons [13, 14], to the best of our knowledge, no investigation about the optical Kerr effect in the evanescent field of an optical nanofiber has been reported yet.

In this paper, we report on a theoretical investigation of the optical Kerr effect in silica nanofiber immersed in several nonlinear liquids such as ethanol, acetone and water and we further compare them with air cladding. We provide analytical formula of the effective nonlinear coefficients including the contribution of the evanescent field for varying nanofiber diameter. It is shown for instance that the evanescent field contribution to the total Kerr effect using acetone liquid is greater than that of the silica core for a nanofiber diameter smaller than 560 nm. Furthermore, the

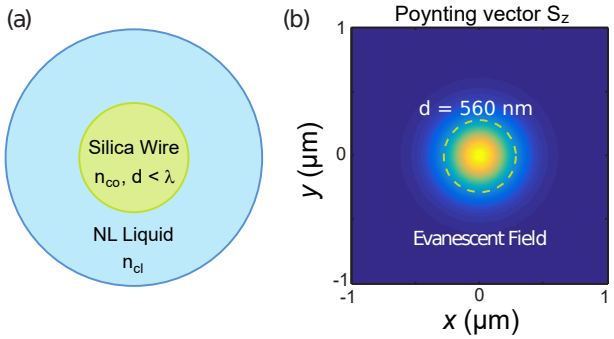

Fig. 1. (a) Scheme of a subwavelength-diameter optical nanofiber immersed in a nonlinear liquid for observing the evanescent Kerr effect. (b) Numerical simulations of the fundamental mode for a nanofiber with a core diameter of 560 nm and immersed in acetone. The dashed line corresponds to the core surface.

experimental evidence of the evanescent Kerr effect (EKE) is reported through the observation of the stimulated Raman-Kerr scattering (SRKS) using an acetone-immersed optical nanofiber.

2. Theoretical model

Figure 1 schematically shows the concept of the evanescent Kerr effect in a liquid-immersed optical nanofibers with cylindrical geometry. The conditions for enhancing the optical Kerr effect using the evanescent field are twofolds. Firstly the nonlinear liquid ~~should~~ have a lower refractive index than silica for mode guidance. Secondly, the silica core ~~should~~ be as small as possible to get the widest evanescent field that can nonlinearly interact with the Kerr liquid. Then the objective is to demonstrate that the evanescent contribution is greater than the core contribution. As a starting point, let us recall that the optical Kerr effect in a nonlinear optical waveguide is usually defined using the following nonlinear parameter

$$\gamma = \frac{2\pi n_2}{\lambda A_{eff}} \tag{1}$$

where n_2 is the nonlinear Kerr index of the nonlinear medium, A_{eff} the effective area of the guided mode, and λ the wavelength of the field propagating in the waveguide. For a tapered fiber with a waist smaller than the optical wavelength, the evanescent field of the fundamental mode which interacts with the external environment becomes more important than that the electric field guided into the core. To include the evanescent field into the Kerr effect, we can write the effective nonlinear parameter γ_{eff} for a mode as [15]:

$$\gamma_{eff} = \frac{2\pi}{\lambda} \frac{\iint_{-\infty}^{+\infty} n_2(x,y) S_z^2 dxdy}{\left(\iint_{-\infty}^{+\infty} S_z dxdy\right)^2} \tag{2}$$

where S_z is the Poynting vector component in the waveguide direction. We note however that this equation is an approximation as it does not assume the z field component that is no more negligible for very small diameter [1, 15]. However, although the propagating modes of a waveguide are not fully transverse in strong guidance regime, it has been shown that the full vectorial formalism of γ_{eff} and the simplified expression of Eq. 2 gives the same results of γ_{eff} for silica nanofiber in air even for small core diameter down 0.3 ~~Âtm~~ [15]. As the core-cladding index difference decreases when liquids surround the nanofiber, Eq. 2 thus remains

	silica core	air	water	ethanol	acetone
n_0	1.4606	1	1.3337	1.3637	1.3614
n_2	2.6	3.10^{-3}	4.1	7.7	24

Table 1. Refractive indices n_0 and Kerr indices n_2 (10^{-20} m^2/W) of air and several nonlinear liquids and for a pump wavelength $\lambda = 532$ nm. The n_0 indices have been calculated using the Sellmeier coefficients. The n_2 coefficients comes from Ref. [16], except for silica. [15].

valid. Assuming a Kerr index n_2 uniform in the core and cladding regions, the expression of γ of Eq. 1 is still valid and the effective area writes as:

$$A_{eff} = \frac{\iint_{-\infty}^{+\infty} S_z^2 dxdy}{\left(\iint_{-\infty}^{+\infty} S_z dxdy\right)^2} \tag{3}$$

If now the core and cladding have different Kerr coefficients, the previous equation 2 can be decomposed as follows:

$$\gamma_{eff} = \frac{2\pi n_{2,co}}{\lambda} \frac{\iint_{co} S_z^2 dxdy}{\left(\iint_{-\infty}^{+\infty} S_z dxdy\right)^2} + \frac{2\pi n_{2,cl}}{\lambda} \frac{\iint_{cl} S_z^2 dxdy}{\left(\iint_{-\infty}^{+\infty} S_z dxdy\right)^2} \tag{4}$$

with $n_{2,co}$ and $n_{2,cl}$ the core and cladding Kerr coefficient, respectively, considered as uniform. Then, the first term of Eq. 4 corresponds to the contribution to the Kerr effect of the silica core of the nanofiber, whereas the second term corresponds to the contribution of the cladding of the nanofiber. These two contributions can be independently computed and then summed as $\gamma_{eff} = \gamma_{co} + \gamma_{cl}$.

Table 1 gathers the linear and nonlinear refractive indices, n_0 and the n_2, of the different media used in our model, and for a pump wavelength of $\lambda = 532$ nm [15, 16]. Although acetone seems to be the best candidate for increasing the Kerr nonlinearity, we have investigated different liquids for the sake of comparison. Indeed, ethanol and acetone have nearly the same refractive index but different Kerr coefficients. The comparison will allow us for estimating the sensitivity of the nonlinear parameter to the Kerr coefficient of the liquids. On the other hand, water and ethanol (or acetone) will be used to compare two liquids with different refractive indices and nonlinear Kerr coefficients with opposite behavior about the Kerr effect. The results of this paper will therefore be helpful in estimating the effective Kerr parameter γ_{eff} for other nonlinear liquids. To get the effective Kerr coefficient, we first computed the electric and magnetic fields of the fundamental mode using a finite element method (FEM, COMSOL Multiphysics). A perfectly matched layer (PML) with cylindrical symmetry has also been included in the numerical method to absorb light at open boundaries and to estimate the loss of all the spatial modes. This provides further information about the modal properties, single-mode guidance conditions, and linear attenuation. The results show that fundamental mode is guided lossless at 532 nm for diameters ranging from 0.3 μm up to 0.8 μm and using most surrounding media, except with ethanol and acetone for diameter smaller than 0.35 μm because there is no guided mode. From the computed fields, we then calculated a number of parameters including the effective Kerr coefficient γ_{eff}, the effective area of the fundamental mode A_{eff}, the fraction of intensity in the evanescent field $f = \frac{\iint_{cl} S_z dxdy}{\iint_{-\infty}^{+\infty} S_z dxdy}$, the contributions to the Kerr parameter of the silica core γ_{co} and of the cladding γ_{cl}, respectively. The ratio γ_{cl}/γ_{eff} was further derived to quantify the cladding

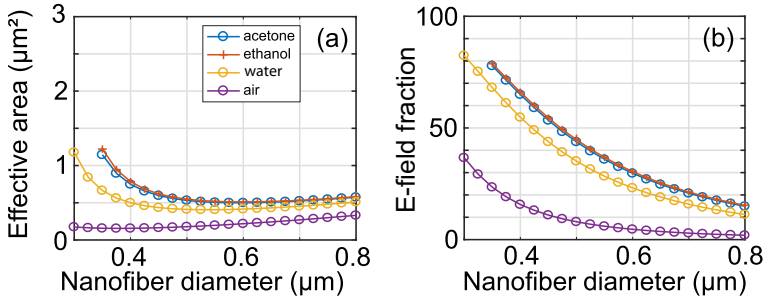

Fig. 2. (a) Effective mode area as a function of the nanofiber diameter for air cladding and different nonlinear liquids, (b) Fraction of power density in the evanescent field for an optical wavelength λ=532 nm.

contribution in the effective Kerr parameter.

3. Numerical results and discussion

Figures 2 (a-b) show the effective area A_{eff} of the fundamental mode and the evanescent field fraction f for an increasing diameter d from 0.3 to 0.8 μm and using different claddings (air, water, ethanol, acetone). For a given diameter, we can see that the effective area increases when decreasing the index step Δn between core and cladding, from air to ethanol. When varying the nanofiber diameter, the effective mode area decreases till a minimum value before increasing for diameters lower than the wavelength. This means that the mode field extends spatially while increasing its evanescent part outside the silica core [3, 4]. This leads to this minimum effective area and this depends on the index step Δn. From Fig. 2 (a), we find that the fiber diameter for the smallest effective area is d = 350 nm, 525 nm, 590 nm, and 580 nm for cladding of air, water, ethanol and acetone, respectively. Figure 2(b) further shows that an evanescent field fraction of 50% is reached for diameter smaller than d = 421 nm, 472 nm and 467 nm using as a cladding water, ethanol and acetone, respectively, while this threshold can never be reached for the air-clad nanofiber, due to the larger index step Δn in air compared to the other liquids.

In Figs. 3(a-d), we plotted the nonlinear parameter contribution of the silica core γ_{co} and of the cladding γ_{cl}, the effective nonlinear coefficient γ_{eff} and the evanescent Kerr rate, all in function of the nanofiber diameter. Concerning the silica core contribution γ_{co}, we can see that this parameter dramatically changes when using liquids as cladding compared to air. It first increases until reaching a maximum value for diameters close to those of the minimal effective area (See Figure. 2(a)). This is due to the fact that if the effective mode area is very weak, the field intensity and therefore the Kerr effect in the silica core are maximum. Consequently, the ascending order of the γ_{co} follows the descending order of the effective area or of the refractive index step for the different external media. Then, it is clear that γ_{co} is strongly greater for nanofiber in air than in liquids, in agreement with Fig. 3(a). For small diameters, the core contribution drastically decreases and tends to zero since the fundamental mode spreads out spatially with increasing mode effective area. Concerning the cladding contribution (Fig. 3(b)), the evolution is nearly similar. Since the intensity fraction in the evanescent field increases (Fig. 2(b)) with decreasing nanofiber diameter, γ_{cl} increases up to reach a maximum and to decrease thereafter. This peak value corresponds to an optimal balance between the increase of the evanescent field that gives rise to the Kerr effect enhancement and to the decrease of the field intensity. This peak value is achieved for diameter lower that those for minimal effective area. For a given nanofiber diameter, the dependence of γ_{cl} on the cladding materials follows the order of their Kerr indices : the higher the Kerr index is, the stronger the gamma parameter is. However, the ratio between two γ_{cl} for two different media depends not only on the ratio of the respective Kerr coefficients n_2

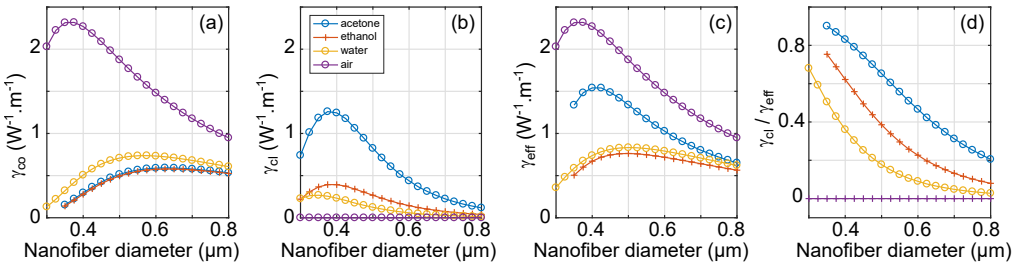

Fig. 3. Evolution in function of the nanofiber diameter and for different surrounding media of (a) the nonlinear parameter contribution of the silica core γ_{co} (b) the nonlinear parameter contribution of the cladding γ_{cl}, (c) the whole effective nonlinear parameter γ_{eff}, and (d) the γ_{cl}/γ_{eff} ratio. The optical wavelength is λ = 532 nm.

of the media but also on the fraction of the evanescent field, i.e., on the refractive indices ratio between the liquids. Therefore, for acetone and ethanol, the γ_{cl} ratio is almost equivalent to their n_2 ratio as their refractive indices are very close. This is however not the case for acetone and water. Figure 3(c) shows the effective Kerr parameter $\gamma_{eff} = \gamma_{co} + \gamma_{cl}$. First of all, it is clear that the Kerr parameter γ_{eff} remains maximum for a nanofiber in air, even if the contribution of the evanescent field to the Kerr effect is null, and even compared to a nanofiber immersed in acetone which presents the highest Kerr coefficient n_2. This is due to the fact that the effective area of the fundamental mode for a nanofiber in air remains the smallest, leading to high field intensity and Kerr effect. The parameter γ_{eff}, for the core contribution γ_{co}, has a maximum value of 2.3 W^{-1}.m^{-1} for a small diameter d = 375 nm.

Although γ_{eff} is lower for a nanofiber immersed in a liquid, the contribution of the evanescent field to the Kerr effect may be comparable or even higher than that from the silica core. This is shown when comparing Fig. 3(a) to Fig. 3(b). For acetone, γ_{eff} has a maximal value of 1.54 W^{-1}.m^{-1} for a core diameter of d = 410 nm. For that diameter, γ_{cl} = 1.22 W^{-1}.m^{-1} and γ_{co} = 0.32 W^{-1}.m^{-1}. Therefore, almost 80% of the Kerr parameter is in the evanescent field. We note from this analysis that this large evanescent fraction is no more correlated to the effective area of the mode which is minimum for a nanofiber diameter of d = 580 nm. The relationship $\gamma = \frac{2\pi n_2}{\lambda A_{eff}}$ is therefore no longer valid for a nanofiber immersed in a liquid when the evanescent part of the field becomes significant.

If we now compare the role of ethanol and acetone that have the same effective mode area (Fig. 2(b)), the contribution γ_{co} is therefore equivalent for both liquids (Fig. 3(b)). In addition, as the Kerr coefficient n_2 of acetone is higher than that of ethanol, the contribution γ_{cl} is clearly greater for acetone. Thus, the effective Kerr coefficient is about 2 times larger for acetone than ethanol. The same analysis can be performed when comparing water and ethanol. The core contribution γ_{co} for a nanofiber in water is higher than that of a nanofiber in ethanol as its step refractive index is the lowest. Consequently, a nanofiber in water will have a lower evanescent field than in ethanol (Fig. 2(b)). However, water has a lower Kerr coefficient than ethanol, leading to a highest cladding contribution γ_{cl} in ethanol. These two contributions have opposite sign and give rise to similar nonlinear parameters γ_{eff} for both liquids (Fig. 3(c)).

~~By comparing~~ Fig. 3(d) and Fig. 2(b), ~~it is clear~~ that the evolution of the contribution of the evanescent field to the Kerr effect is not identical to that of the outer fraction of the field. The reason for that behavior is that the Kerr effect is not only related to the spatial extent of the electric field but also to the Kerr coefficient of the nonlinear liquid. Thus, for a nanofiber in acetone, the ratio γ_{cl}/γ_{eff} reaches 50% for a nanofiber diameter ~~equal to~~ d = 560 nm, while the outer fraction of the field is only 39 %. This difference is shown in Fig. 4. This figure represents the 2D spatial profile ~~for~~ the γ_{eff} ~~global~~ parameter for a core diameter of 560 nm, as ~~for~~ Fig. 1(b). We

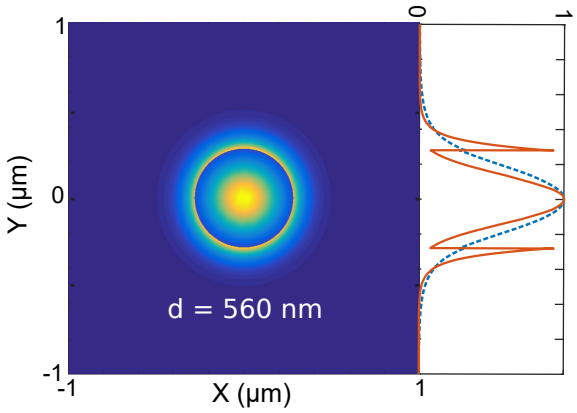

Fig. 4. 2D spatial profile of the γ_{eff} ~~global~~ parameter. Right window: Y-cut spatial profile of the Poynting vector (blue dotted curve) of Fig. 1(b), and of the γ_{eff} parameter (orange curve).

clearly observe the increase of the γ_{eff} in the liquid. Moreover, the right window represents the normalized profile along the Y axis of the Poynting vector (blue dotted curve) shown in Fig. 1(b), and of the γ_{eff} parameter (solid orange curve). It is clear that the Kerr effect is enhanced in the liquid, with a maximal spatial extension of about 150 ~~Âţm~~ around the nanofiber.

It is noteworthy that ~~EKE presents several origins~~, according to the considered medium, with different time scales for the nonlinear response in function of the origin of the nonlinear change in the refractive index. Thus, the electronic polarization of liquids and silica is associated to an instantaneous response, whereas the liquid molecule reorientations lead to several non instantaneous responses with picosecond time scales [17].

4. Experimental observation

Experimentally, the evanescent Kerr effect can be observed using different ways. The first one is the self-phase modulation (SPM) which gives rise to a spectral broadening of the pump laser pulse scaling with to the γ_{eff} parameter [18]. However, the theory predicts that the total Kerr effect, and therefore the SPM-induced spectral broadening, will decrease in an air-clad nanofiber compared to a liquid-clad nanofiber mainly because of absorption. It seems thus difficult to experimentally demonstrate the evanescent Kerr effect by comparing the SPM-induced spectral broadening in liquids and air. This quantitative approach is delicate to implement, and anyway, it does not prove the presence of EKE as this latter is mixed with the core contribution to the Kerr effect. Another experimental approach that would allow for the observation of the evanescent Kerr effect is based on using stimulated Raman-Kerr scattering (SRKS). This inelastic light scattering comes from the inertial nature of reorientation motion of anisotropic molecules of many liquids, as those used in this study, and it gives rise to a broad asymmetric broadening of the Raman Stokes spectrum towards the red [19–23]. It can be understood as follows: unlike the case of gaseous medium, molecules in liquid phase cannot rotate freely due to viscosity. To make a re-orientational motion within a liquid, a molecule has to get more energy to overcome the viscosity, leading to inelastic light scattering over a broad Stokes frequency range beyond the initial Raman frequency shift. A broadening on the anti-Stokes side due to the thermal collisions between molecules that promote this re-orientational motion can also be observed [19]. This broadening is more important when the temperature of the liquid is high, while generally remaining lower than the Stokes broadening. It is important to note that SRKS process needs a long interaction length between liquid and light to be significantly observed. Moreover, as

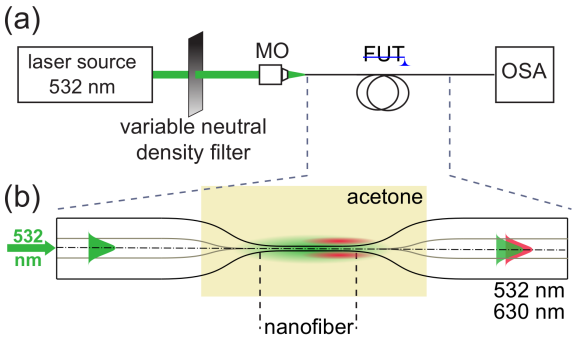

Fig. 5. (a) experimental setup. MO microscope objective X10, ~~FUT fiber under test~~, OSA optical spectrum analyser. (b) Detailed scheme of the nanofiber, with the spectral component generated with the pump evanescent field by stimulated Raman scattering in acetone.

this process depends on the random initial orientation of the molecules, ~~and corresponds to a stochastic process,~~ the SRKS ~~spectral components~~ are not coherent. Therefore, if we could observe SRKS on the Stokes and anti-Stokes sides of the Raman lines of liquids, this would mean that the evanescent nonlinearities as Raman and inertial Kerr effects are simultaneously present in the liquids. This is shown experimentally in Figure 6. The experimental setup is drawn in Fig. 5(a). In our experiment, we made a single-mode silica nanofiber using the heat-brush technique described in Ref. [24]. It has a uniform diameter of 580 nm over a 4 cm length and the two transition tapers are 8 *cm* long. As a laser source, we used a frequency-doubled Nd:YAG laser at 532 nm with a repetition rate of 21 kHz and delivering Gaussian pulses of 500 ps of duration (FWHM) (Fig. 5(a)). A detailed scheme of the nanofiber immersed in acetone is shown in Fig. 5(b). The pump evanescent field is drawn around the nanofiber, such as the Raman spectral component generated along the nanofiber in the acetone by the evanescent part of the pump field. Figure 6 shows the experimental spectra at the fiber output of the nanofiber when increasing the input mean power from 4 to 15 mW. The spectral components correspond to the Raman lines with the highest gain due to vibration of acetone molecules with the Raman shift of 2925 cm^{-1} [25]. The first Raman order is generated around 630 nm. When the input power increases, the Raman cascading process occurs and the second Raman order is generated at 772.5 nm. Moreover, a spectral broadening of the first Raman peak increases with the input pump power due to the SRKS process. Indeed, the pump spectrum does not present simultaneously a broadening that could justify this observation. Moreover, the second Raman order presents a narrow linewidth proving that it is generated by the coherent part of the first Raman order, behavior already observed in Ref. [23]. Note that a significant broadening on the anti-Stokes side appears, certainly due to the high temperature close to the nanofiber. To resume, as the broadening in the Stokes side due to SRKS is clearly visible when the input pump power increases, the Kerr effect then occurs in the liquid which clearly demonstrates the presence of evanescent Kerr field. It is noteworthy that this is the first time to our knowledge that SRKS phenomenon is observed in acetone, and also that SRKS occurs over a so weak interaction length. Note that the Raman effect in acetone appears clearly before the Raman effect in silica, showing that evanescent Raman scattering is very efficient in comparison with Raman effect in silica core due to the gap between their Raman gain coefficients.

5. Conclusion

In summary, we theoretically and experimentally investigated the optical Kerr effect in the evanescent field of a silica nanofiber surrounded by nonlinear liquids such as water, ethanol

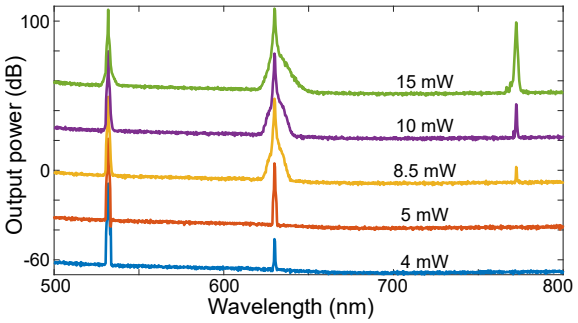

Fig. 6. Experimental measurements, output spectra as a function of input mean pump power showing the stimulated Raman-Kerr scattering induced by the evanescent field in an acetone-immersed silica nanofiber.

and acetone. We have shown that the effective Kerr coefficient contains two contributions: the contribution of the silica core which depends on the diameter of the nanofiber and follows the inverse of the effective area, and the contribution of the cladding via the evanescent field which depends on the diameter of the nanofiber and the nonlinear properties of the external environment. It has been further shown that the contribution to the optical Kerr effect in the evanescent field of the fundamental mode overpasses that of the core when the nanofiber is immersed in a highly nonlinear liquid such as acetone for diameter below 560 nm. A detailed comparison with air and other liquids was further provided and we reported the evidence of the evanescent Kerr effect via the observation of the Stimulated Raman-Kerr scattering in the evanescent field. The evanescent Kerr and Raman effects shown in here may find potential applications to ultra-sensitive liquid sensing and Raman spectroscopy, as the optical mode propagating in the optical nanofiber essentially interacts with the outer environment without any major contribution from the nanofiber.

Funding

This project has received funding from the Agence Nationale de la Recherche (ANR) (ANR-16-CE24-0010; ANR-15-IDEX-0003, ANR-17-EURE-0002) and the European union H2020 program MSCA-ITN-SUPUVIR under grant agreement 722380, and the Conseil Regional de Bourgogne Franche-Comte.

References

1. L. Tong and M. Sumetsky, "Subwavelength and nanometer diameter optical fibers," Springer, 978-3-642-03362 (2011).
2. L. Tong, R. R. Gattass, J. B. Ashcom, S. He, J. Lou, M. Shen, I. Maxwell and E. Mazur, Nature **426**, 816âĂŞ819 (2003).
3. L. Tong, J. Lou, and E. Mazur, Opt. Express **12**, 1025âĂŞ1035 (2004).
4. M. A. Foster, A. C. Turner, M. Lipson, and A. L. Gaeta, Opt. Express **16**, 1300–1320 (2008).
5. G. Brambilla, "Optical fiber nanowires and microwires: a review," J. Opt. **12**, 043001 (2010).
6. T. A. Birks, W. J. Wadsworth, and P. St. J. Russell, Opt. Lett. **25**, 1415-1417 (2000).
7. C. Wuttke, M. Becker, S. Brückner, M. Rothhardt, and A. Rauschenbeutel, "Nanofiber Fabry–Perot microresonator for nonlinear optics and cavity quantum electrodynamics," Opt. Lett., **37**, 1949–1951 (2012).
8. M. J. Morrissey, K. Deasy, M. Frawley, R. Kumar, E. Prel, L. Russell, V. G. Truong, and S. N. Chormaic. Sensors **13**, 10449-10481 (2013).
9. W. Talataisong, R. Ismaeel, and G. Brambilla, Sensors **18**, 461 (2018).
10. S. M. Spillane, T. J. Kippenberg, O. J. Painter, and K. J. Vahala, "Ideality in a Fiber-Taper-Coupled Microresonator System for Application to Cavity Quantum Electrodynamics", Phys. Rev. Lett. **91**, 043902 (2003).
11. J.-C. Beugnot, S. Lebrun, G. Pauliat, H. Maillotte, V. Laude, and T. Sylvestre, "Brillouin light scattering from surface acoustic waves in a subwavelength-diameter optical fibre", Nat. Commun. **5**, 5242 (2014).
12. L. Shan, G. Pauliat, G. Vienne, L. Tong, and S. Lebrun, Appl. Phys. Letters **102**, 201110 (2013).

13. J. M. Vigoureux and D. Courjon, "Evanescent Wave Mixing on Nonlinear Surfaces," Journal of Modern Optics **36**(12):1575-1580 (2007).
14. J. Renger, R. Quidant, N. van Hulst, and L. Novotny, "Surface-Enhanced Nonlinear Four-Wave Mixing," Phys. Rev. Lett. **104**, 059903 (2010).
15. S. Afshar V., and T. M. Monro, Opt. Express **17**(4), 2298-2318 (2009).
16. R. W. Boyd, *nonlinear optics*, Academic Press, 3rd Ed. (2008).
17. M. Reichert, H. Hu, M. Ferdinandus, M. Seidel, P. Zhao, T. Ensley, D. Peceli, J. Reed, D. Fishman, S. Webster, D. Hagan, and E. Van Stryland, Optica **1**(6), 436–445 (2014).
18. G. Agrawal, *Nonlinear fiber optics*, Academic Press, 5th Ed. (2013)
19. G. S. He, and P. N. Prasad, "Stimulated Kerr scattering and reorientation work of molecules in liquid CS_2", Phys. Rev. A **41**, 2687–2697 (1990).
20. G. S. He, R. Burzynski, and P. N. Prasad, "A novel nonlinear optical effect: Stimulated Raman–Kerr scattering in a benzene liquid–core fiber", J. Chem. Phys. **93**, 7647–7655 (1990).
21. G. S. He and P. N. Prasad, "Stimulated Rayleigh-Kerr and Raman-Kerr Scattering in a Liquid–Core Hollow Fiber System", Fiber Integr. Opt. **9**, 11-26 (1990).
22. G. Fanjoux, A. Sudirman, J.-C. Beugnot, L. Furfaro, W. Margulis, and T. Sylvestre, Opt. Lett. **39**, 5407–5410 (2014).
23. G. Fanjoux, S. Margueron, J. Beugnot, and T. Sylvestre, J. Opt. Soc. Am. B **34**, 1677–1683 (2017).
24. A. Godet, A. Ndao, T. Sylvestre, V. Pecheur, S. Lebrun, G. Pauliat, J.-C. Beugnot, and K. P. Huy, "Brillouin spectroscopy of optical microfibers and nanofibers," Optica, **4**, 1232–1238 (2017).
25. A. Laubereau and R. Laena, *Ultrafast Infrared and Raman Spectroscopy*, Ed. by M. D. Fayer (CRC Press, 2001).